

Numerical Study of the Spin Hall Conductance in the Luttinger Model

W.Q. Chen¹, Z.Y. Weng¹, and D.N. Sheng²

¹*Center for Advanced Study, Tsinghua University, Beijing 100084*

²*Department of Physics and Astronomy, California State University, Northridge, CA 91330*

We present first numerical studies of the disorder effect on the recently proposed intrinsic spin Hall conductance in a three dimensional (3D) lattice Luttinger model. The results show that the spin Hall conductance remains finite in a wide range of disorder strength, with large fluctuations. The disorder-configuration-averaged spin Hall conductance monotonically decreases with the increase of disorder strength and vanishes before the Anderson localization takes place. The finite-size effect is also discussed.

A primary goal of spintronics is to make use of spin degree of freedom of electrons in the future ‘electronic’ devices [1, 2]. The spin Hall effect (SHE) may be one of potentially effective ways to manipulate the spin transport. An extrinsic SHE generated by impurities with spin-orbit (SO) coupling has been previously proposed [3]. By scattering electrons of different spins into different directions, a net spin current can be established in the transverse direction, accompanying the charge current induced by an applied electric field. But usually the resulting spin accumulation is very weak as it crucially depends on the impurity concentration. Recently, a much stronger SHE due to the intrinsic SO coupling in clean materials has been proposed for both the 3D p-doped semiconductors described by the Luttinger model [4], and the two-dimensional (2D) electron gas described by the Rashba model [5]. Here it has been argued that the ‘dissipationless’ spin currents can be of several orders of magnitude larger than in the case of the extrinsic SHE. A signature of spin polarization observed recently in the 2D hole gas (2DHG) [6] and 3D n-doped semiconductors [7] might be originated from the intrinsic SHE [8, 9].

However, the effect of disorder on the intrinsic SHE remains a highly controversial issue so far. It has been argued [10, 11] that the spin current in the 2D Rashba model should vanish, even in the weak disorder limit, after considering the vertex corrections. On the other hand, it is shown that the vertex correction vanishes for the Luttinger [12] and 2DHG [8] models such that the SHE is robust in the latter models at least when disorders are weak. Clearly disorder effect is nonperturbative on the spin Hall transport properties, and numerical approaches are highly desirable in order to illustrate the fate of spin Hall conductance (SHC) in disordered systems. So far there have been a series of numerical works dealing with the SHE in the presence of disorders in the 2D Rashba model [13, 14, 15, 16]. These calculations suggest that the SHC survives finite length scales in disordered systems with indications of its vanishing in the thermodynamic limit. To our knowledge no numerical work has been done in the 3D Luttinger model with regard to the disorder effect.

of the SHC in the lattice Luttinger model with including an on-site random potential based on the Kubo formula. We find that the SHC at weak disorder is intrinsically fluctuating, similar to the quantum Hall state around the critical point. The distribution of the SHC over different disorder configurations shows a strong symmetric peak with the averaged SHC located at the peak position. The averaged SHC remains finite in a wide range of disorder strengths covering the main regime of the metallic phase while the finite-size scaling analysis suggests that SHC can survive at larger length scales. The calculated SHC decreases monotonically with increasing disorder strength, and disappears not far before the 3D Anderson localization takes place.

We start with the tight-binding version of the 3D Luttinger Hamiltonian, which can be derived from the continuum version [4] with using the replacement $k_\nu \rightarrow \sin k_\nu$ and $k_\nu^2 \rightarrow 2(1 - \cos k_\nu)$. After a discrete Fourier transformation, the resulting Hamiltonian reads

$$\begin{aligned}
 H = & - \sum_{\langle ij \rangle} (c_i^\dagger c_j + h.c.) + V_L \sum_{i,\nu} (c_i^\dagger S_\nu^2 c_{i+\nu} + h.c.) \\
 & + \frac{V_L}{8} \sum_{i,\mu \neq \nu} c_i^\dagger \{S_\mu, S_\nu\} (c_{i+\mu+\nu} + c_{i-\mu-\nu} \\
 & - c_{i+\mu-\nu} - c_{i-\mu+\nu}) + \sum_i \epsilon_i c_i^\dagger c_i
 \end{aligned} \quad (1)$$

where the electron annihilation operator c_i has four components characterized by the ‘spin’ index $S_z = \frac{3}{2}, \frac{1}{2}, -\frac{1}{2}, -\frac{3}{2}$, respectively, and $i + \nu$ ($\nu = x, y, z$) denote the nearest-neighbors of site i , and $i + \nu + \mu$, etc., for the next nearest-neighbor sites. Here $V_L \equiv \frac{2\gamma_2}{\gamma_1 + \frac{3}{2}\gamma_2}$ represents the strength of the Luttinger spin-orbital coupling. We choose $V_L = 0.364$ as the ratio γ_1/γ_2 is around 3 in typical semiconductors [17]. The last term accounts for on-site nonmagnetic disorder with ϵ_i randomly distributed within $[-W/2, W/2]$. Note that the Luttinger model is only a valid description of real semiconductors around the Γ points at $k_\nu \rightarrow 0$, which corresponds to choosing the Fermi energy near the band edge in the present tight-binding version.

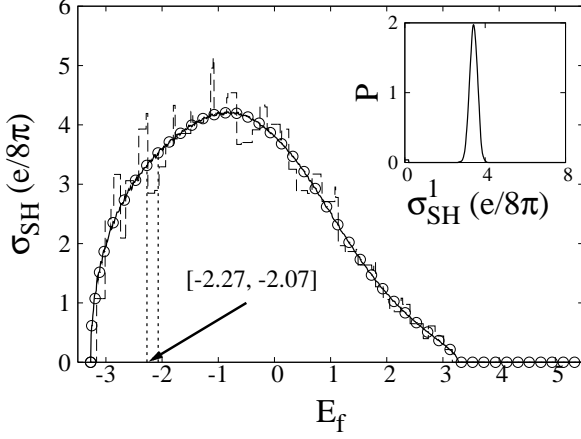


FIG. 1: σ_{SH} vs the Fermi energy E_f in the pure system. The dashed curve is for $8 \times 8 \times 8$ lattice and the solid one is for $50 \times 50 \times 50$ lattice with PBC. The open circles for $8 \times 8 \times 8$ lattice are obtained by averaging over 200 configurations of different BCs, which coincide with the solid curve very well. The inset shows $P(\sigma_{SH}^1)$, defined as the distribution of the spin Hall conductance, at $8 \times 8 \times 8$ under different BCs with E_f 's within the range indicated by the arrow in the main panel.

lated by the Kubo formula[18]

$$\sigma_{SH}^1 = -\frac{2}{N_L} \text{Im} \sum_{E_n < E_f < E_m} \frac{\langle n | j_x^{y\text{spin}} | m \rangle \langle m | j_z | n \rangle}{(E_m - E_n)^2}, \quad (2)$$

in which N_L is the number of lattice sites, E_f denotes the Fermi energy, $E_{m,n}$ is the eigen-energy, the charge current operator $\mathbf{j} = e\mathbf{v}$ and the spin current $\mathbf{j}_\mu^{\text{spin}} = \frac{1}{2}\{v_\mu, S_\nu\}$. Here the velocity operator \mathbf{v} as the conjugate operator of the position operator $\mathbf{R} \equiv \sum_{i\sigma} \mathbf{r}_i n_{i\sigma}$ ($n_{i\sigma}$ is the number operator at site i with spin index σ), is defined by the standard relation $\mathbf{v} = \frac{i}{\hbar}[H, \mathbf{R}]$. In the presence of random disorder $W \neq 0$, the SHC is obtained by averaging σ_{SH}^1 over all disorder configurations, *i.e.*,

$$\sigma_{SH} = \langle \sigma_{SH}^1 \rangle. \quad (3)$$

In a finite-size calculation, a proper boundary condition (BC) is necessary for diagonalizing the Hamiltonian. A general (twisted) BC, *e.g.*, $\psi(x + L_x, y, z) = e^{2\pi i \phi_x} \psi(x, y, z)$, etc., where L_x is the sample size along the x -direction, and ϕ_x is defined within $[0, 1]$ with $\phi_x = 0$ corresponding to the periodic BC (PBC) along this direction. In the thermodynamic limit, a physical quantity should not depend on BCs. In a finite-size calculation, the BC averaging can be very **effective** in smoothening out finite-size fluctuations in σ_{SH} in a spin-orbit coupling system [16]. In principle, this procedure is not necessarily the unique one for a finite system (as one can also use the fixed BCs in the calculation), but smoother data obtained this way can allow one to make a finite-size scaling analysis and to meaningfully extrapolate the results

consider the PBC in the pure system with $\epsilon_i = 0$. The calculated σ_{SH} for a $8 \times 8 \times 8$ lattice is shown in Fig. 1 by the dashed curve, which quickly fluctuates, as a function of E_f , with finite steps due to the finite-size effect. Such a finite-size effect disappears when the sample size is increased to $50 \times 50 \times 50$ (this size can only be reached for the pure system, where the momentum is a good quantum number, in our calculation) with the same PBC, as indicated by the smooth solid curve in Fig. 1. On the other hand, if one averages over different BCs (over 200 configurations) in Eq. (3) for the $8 \times 8 \times 8$ lattice, the steps in the dashed curve can also become smoothened out as represented by the open circles which coincide very well with the solid curve obtained for the bigger lattice of $50 \times 50 \times 50$ in Fig. 1.

The fluctuations in σ_{SH}^1 become very large in the presence of disorders, typically in a range of 5-10 times larger than the averaged value. To quantitatively describe such fluctuations, we shall introduce the so-called distribution of the SHC (DSHC), $P(\sigma_{SH}^1)$, which determines the averaged SHC, σ_{SH} , by

$$\sigma_{SH} = \int d\sigma_{SH}^1 P(\sigma_{SH}^1) \sigma_{SH}^1. \quad (4)$$

First, for a given E_f , we can calculate σ_{SH}^1 at different disorder and BC configurations within a small Fermi energy interval, say, $[-2.27, -2.07]$ around $E_f = -2.17$ as illustrated in Fig. 1 by the arrow [here the change in $\sigma_{SH}(E_f)$ is presumably weak as a function of E_f]. Suppose that the total number of computed σ_{SH}^1 's is N in this range, and the number of σ_{SH}^1 's at $\sigma_{SH}^1 = \sigma \pm \Delta\sigma$ [$\Delta\sigma = \pm 0.01$ ($e/8\pi$)], is denoted by $\Delta N(\sigma)$. Then the DSHC is defined as the statistic distribution of σ_{SH}^1

$$P(\sigma) = \frac{\Delta N(\sigma)}{N \Delta\sigma}. \quad (5)$$

The DSHC for the pure system of a $8 \times 8 \times 8$ lattice for 200 different BCs is shown in the inset of Fig. 1, in which $P(\sigma)$ is a very symmetric peak such that one may simply use the peak position, $\frac{3.4e}{8\pi}$, to determine the averaged σ_{SH} instead of directly evaluating the average in Eq.(4). A similar technique has been used in the quantum Hall effect system [19].

Fig. 2 (a) shows the DSHC at $W = 3$ for a $6 \times 6 \times 6$ lattice, with the Fermi energy E_f fixed as the same value as in Fig. 1. Here the open squares correspond to the result obtained over $N = 1000$ configurations of random disorder and BCs, while the closed squares are for the $N = 5000$ configurations. Clearly the DSHC becomes smoother with the increase of N , whose symmetric peak position remains unchanged with essentially the same envelop. The solid curve in Fig. 2 (a) is obtained by averaging the DSHC at $N = 1000$ over a small range of σ : $[\sigma - \delta, \sigma + \delta]$ with $\delta = 0.2$ ($e/8\pi$), defined by $P(\sigma) = \frac{1}{\delta} \int_{\sigma-\delta}^{\sigma+\delta} P(\sigma') d\sigma'$, which coincides with the data

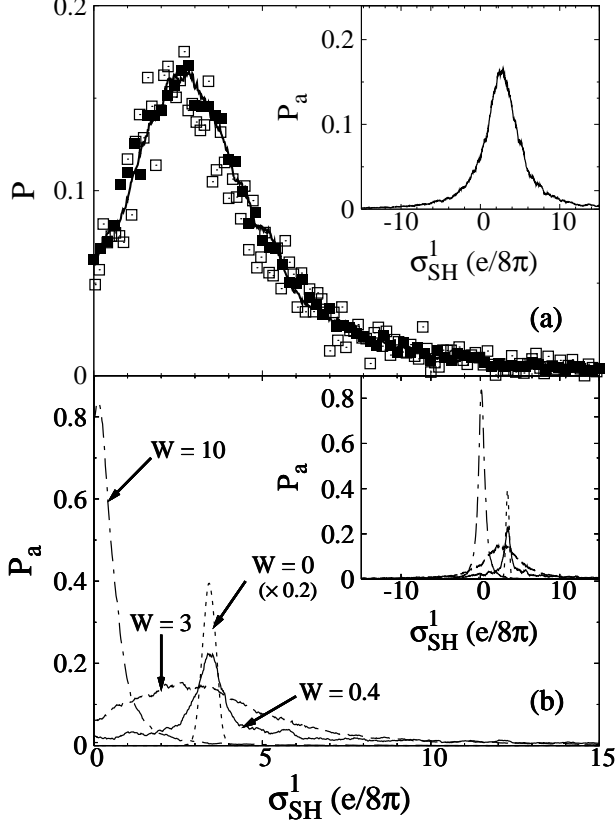


FIG. 2: (a) The DSHC at $W = 3$ on a $6 \times 6 \times 6$ lattice. Open square denotes 1000 random disorder and BC configurations, and the closed square is for 5000 configurations. The solid curve is the averaged DSHC, P_a (defined in the text), at 1000 configurations. The inset shows P_a in a larger scale. (b): P_a at different disorder strengths. The dotted one is for $W = 0$; the solid curve: $W = 0.4$; the dashed curve: $W = 3$; the dash-dot curve: $W = 10$. Inset: the same curves in a larger scale.

at $N = 5000$ very well and is plotted in a wider range of σ in the inset. The calculated P_a at $W = 0, 0.4, 3.0$, and 10 , respectively, for a $8 \times 8 \times 8$ lattice averaged over 200 configurations are presented in Fig. 2 (b). The main panel focus on the neighborhood around the peaks of $P_a(\sigma)$ and the inset illustrates the peaks in a larger scale, whose lineshapes are generally symmetric such that one may read off the value of σ_{SH} directly from the peak position as discussed above.

Now we study the sample-size dependence of the SHC with focusing on three disorder strengths: $W = 0.4$ for the weak disorder regime; $W = 3$ for the intermediate regime; and $W = 10$ for the strong disorder regime. The results for $W = 0.4$ are plotted in Fig. 3 (a) for three different sizes of the lattice: $6 \times 6 \times 6$ with $N = 500$ (the solid curve), $8 \times 8 \times 8$ with $N = 200$ (the dashed), and $10 \times 10 \times 10$ with $N = 200$ (the dotted). In Fig. 3 (b) the difference between the $6 \times 6 \times 6$ and $10 \times 10 \times 10$ lattices

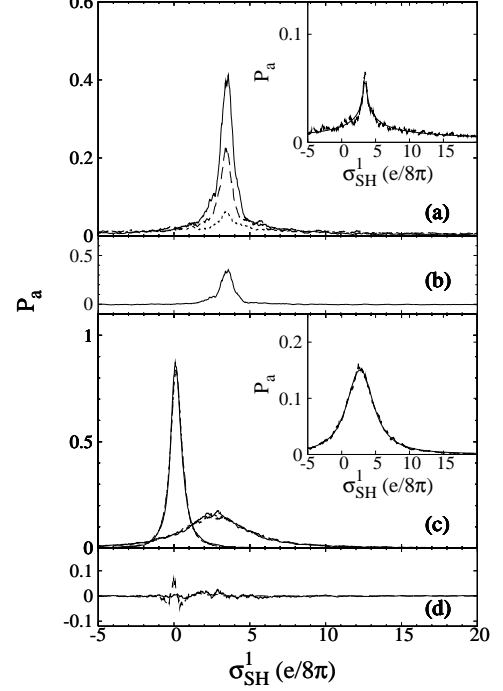


FIG. 3: (a). The DSHC at $W = 0.4$. The solid curve: a $6 \times 6 \times 6$ lattice with 500 configurations, the dashed curve: a $8 \times 8 \times 8$ lattice with 200 configurations and the dotted curve: a $10 \times 10 \times 10$ lattice with 200 configurations. (b). The difference between the DSHCs of sizes $6 \times 6 \times 6$ and $10 \times 10 \times 10$. (c) and (d) are similar to (a) and (b), for $W = 3$ (the right side peak) and $W = 10$ (the left side peak), respectively. The insets in (a) and (c) shows the DSHCs at $10 \times 10 \times 10$ for $W = 0.4$ and 10 , respectively, which are fit by the function $\frac{a}{|\sigma_{SH}^1 - \sigma_{SH}|^{b+c}}$.

unit for all sizes, the P_a at $10 \times 10 \times 10$ has relatively much longer tail such that ΔP_a in Fig. 3(b) remains negative over a wide range of σ_{SH}^1 that is not easily seen by a naked eye. These results show that the peak of $P_a(\sigma_{SH}^1)$ is significantly broadened and reduced with the increase of the sample size, thus the fluctuations may survive in the large system size limit, like near the critical point of quantum Hall system [19]. Such large fluctuations of the SHC may be attributed to the nonconserved spins under the random scattering of disorder. However, the peak position remains essentially unchanged, which still well decides the averaged σ_{SH} . On the other hand, much less sample-size dependence is found for $W = 3$ and $W = 10$, corresponding to two peaks in Fig. 3 (c), respectively, where the data for different sample-sizes all coincide with each other. And the differences of the DSHCs between the $6 \times 6 \times 6$ and $10 \times 10 \times 10$ lattices are shown in Fig. 3 (d) which are indeed much reduced as compared the weak disorder case in (b).

To further characterize the size-dependence of P_a and σ_{SH} , we use a function $\frac{a}{|\sigma_{SH}^1 - \sigma_{SH}|^{b+c}}$ to fit P_a , in which the typical width of the DSHC, $\Delta\sigma_{SH}$, defined as the half width at half maximum (HWHM) is similar to $1/b$ and the

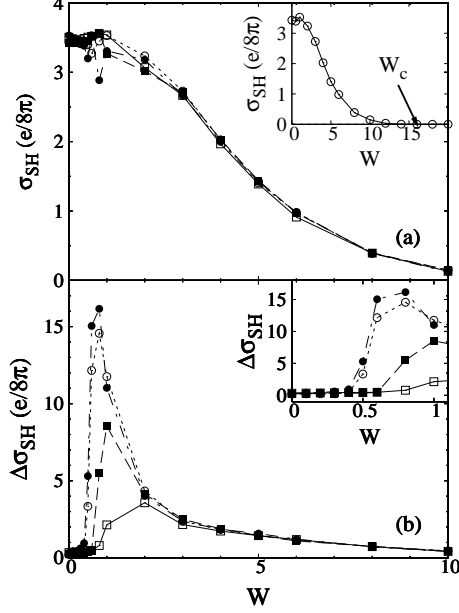


FIG. 4: (a) The W dependence of σ_{SH} . The solid curve with open squares is for $6 \times 6 \times 6$, the dashed curve with close squares is for $8 \times 8 \times 8$, and the dotted curve with open circles is for $10 \times 10 \times 10$, while the dash-dot curve with closed circles is for $6 \times 6 \times 24$. Inset: σ_{SH} over a wider disorder regime, calculated for a $10 \times 10 \times 10$ lattice, where W_c denotes the critical disorder for 3D Anderson localization (see text). (b) The W dependence of the HWHM $\Delta\sigma_{SH}$. The inset shows the details in a weak disorder regime. The notations are the same as in the main panel of (a).

examples of the good fitting are shown in the insets of Fig. 3 (a) and (c) for a $10 \times 10 \times 10$ lattice. In this way we can systematically determine both σ_{SH} and the corresponding $\Delta\sigma_{SH}$ at different sample sizes and disorder strengths. The results are depicted in Figs. 4 (a) and (b) as functions of the disorder strength W . In the weak disorder regime, we see that σ_{SH} remains almost the same as the pure system. With the increase of W , σ_{SH} decreases monotonically and is reduced to 5% of the disorder-free value at $W \sim 10$. It becomes indistinguishable from zero around $W \sim 14$, which is quite close to the typical critical disorder strength, $W_c \sim 16$ [20], of the Anderson localization in 3D systems as marked in the inset of Fig. 4 (a). So the results suggest that the SHE always occurs in the delocalized regime below W_c . Furthermore, the finite-size effect is very weak at $W \geq 2$, from $6 \times 6 \times 6$ to $10 \times 10 \times 10$, with the continuous reduction of $\Delta\sigma_{SH}$ [Fig. 4 (b)].

The overall fluctuations of the SHC and the sample-size dependence are the strongest in the intermediate regime of $0.5 < W < 2$. Both effects are then monotonically reduced at $W \geq 2$, where σ_{SH} becomes weakly dependent on the sample size and the relatively small $\Delta\sigma_{SH}$ is insensitive to the fluctuation of finite-size fluctuations.

larger W . These results suggest that there may exist a characteristic length scale in the spin transport which *decreases* with the increase of W . If this is true, then the extrapolation to the thermodynamic limit should be at least reliable in the strong disorder regime for the present finite-size calculation. By a simple interpolation between the pure case and the strong disorder case, then the SHC is expected to be robust over a wide range of disorder strength.

In conclusion, we numerically studied the distribution of the spin Hall conductance and determine the SHC. The main result shown in Fig. 4 indicates that in the weak disorder regime σ_{SH} remains almost the same as the value for the pure system. With the increase of the disorder strength, σ_{SH} is reduced and terminates before the 3D Anderson localization takes place. Although the calculation has been performed on finite lattice sizes, through the finite-size analysis of the distribution function of the SHC, we found that the results are quite size-independent, suggesting that the SHC in the 3D Luttinger model be robust. This is in contrast to the vanishing behavior found in 2D electron Rashba model, in agreement with analytical results considering vertex corrections[11, 12].

We thank the helpful discussion with S.C. Zhang, M.W. Wu, and C.X. Liu. This work is partially supported by the grants from the NSFC, ACS-PRF 41752-AC10, and the NSF grant/DMR-0307170. The computation of this project was performed on the HP-SC45 Sigma-X parallel computer of ITP and ICTS, CAS.

-
- [1] I. Zutic, J. Fabian, and S. Das Sarma, Rev. Mod. Phys. **76**, 323 (2004).
 - [2] D. D. Awschalom, D. Loss, and N. Samath, *Semiconductor Spintronics and Quantum Computation* (Springer-Verlag, Berlin, 2002).
 - [3] M.I. D'yakonov, and V.I. Perel', JETP Lett. **13**, 467 (1971); J.E. Hirsch, Phys. Rev. Lett. **83**, 1834 (1999).
 - [4] S. Murakami, N. Nagaosa, and S.C. Zhang, Science **301**, 1348 (2003).
 - [5] J. Sinova *et al.*, Phys. Rev. Lett. **92** 126603 (2004).
 - [6] J. Wunderlich, B. Kästner, J. Sinova, and T. Jungwirth, Phys. Rev. Lett. **94**, 047204 (2005).
 - [7] Y. K. Kato, R. C. Myers, A. C. Gossard, and D. D. Awschalom, Science **306**, 1910 (2004).
 - [8] B. A. Bernevig, and S.C. Zhang, cond-mat/0411457; cond-mat/0412550.
 - [9] B. K. Nikolić, S. Souma, L. P. Zârbo, and J. Sinova, cond-mat/0412595.
 - [10] J. Inoue, G. E. W. Bauer, and L. W. Molenkamp, Phys. Rev. B, **70**, 041303(R) (2004).
 - [11] E.G. Mishchenko, A.V. Shytov, and B.I. Halperin, Phys. Rev. Lett. **93**, 226602 (2004).
 - [12] S. Murakami, Phys. Rev. B **69**, 241202(R) (2004).
 - [13] L. Sheng, D.N. Sheng, and C.S. Ting, Phys. Rev. Lett. **84**, 216802 (2000); L. Sheng, D.N. Sheng, and C.S. Ting, Phys. Rev. Lett. **85**, 216802 (2000); L. Sheng, D.N. Sheng, and C.S. Ting, Phys. Rev. Lett. **86**, 216802 (2001); L. Sheng, D.N. Sheng, and C.S. Ting, Phys. Rev. Lett. **87**, 216802 (2002); L. Sheng, D.N. Sheng, and C.S. Ting, Phys. Rev. Lett. **88**, 216802 (2003); L. Sheng, D.N. Sheng, and C.S. Ting, Phys. Rev. Lett. **89**, 216802 (2004); L. Sheng, D.N. Sheng, and C.S. Ting, Phys. Rev. Lett. **90**, 216802 (2005); L. Sheng, D.N. Sheng, and C.S. Ting, Phys. Rev. Lett. **91**, 216802 (2006); L. Sheng, D.N. Sheng, and C.S. Ting, Phys. Rev. Lett. **92**, 216802 (2007); L. Sheng, D.N. Sheng, and C.S. Ting, Phys. Rev. Lett. **93**, 216802 (2008); L. Sheng, D.N. Sheng, and C.S. Ting, Phys. Rev. Lett. **94**, 216802 (2009); L. Sheng, D.N. Sheng, and C.S. Ting, Phys. Rev. Lett. **95**, 216802 (2010); L. Sheng, D.N. Sheng, and C.S. Ting, Phys. Rev. Lett. **96**, 216802 (2011); L. Sheng, D.N. Sheng, and C.S. Ting, Phys. Rev. Lett. **97**, 216802 (2012); L. Sheng, D.N. Sheng, and C.S. Ting, Phys. Rev. Lett. **98**, 216802 (2013); L. Sheng, D.N. Sheng, and C.S. Ting, Phys. Rev. Lett. **99**, 216802 (2014); L. Sheng, D.N. Sheng, and C.S. Ting, Phys. Rev. Lett. **100**, 216802 (2015); L. Sheng, D.N. Sheng, and C.S. Ting, Phys. Rev. Lett. **101**, 216802 (2016); L. Sheng, D.N. Sheng, and C.S. Ting, Phys. Rev. Lett. **102**, 216802 (2017); L. Sheng, D.N. Sheng, and C.S. Ting, Phys. Rev. Lett. **103**, 216802 (2018); L. Sheng, D.N. Sheng, and C.S. Ting, Phys. Rev. Lett. **104**, 216802 (2019); L. Sheng, D.N. Sheng, and C.S. Ting, Phys. Rev. Lett. **105**, 216802 (2020); L. Sheng, D.N. Sheng, and C.S. Ting, Phys. Rev. Lett. **106**, 216802 (2021); L. Sheng, D.N. Sheng, and C.S. Ting, Phys. Rev. Lett. **107**, 216802 (2022); L. Sheng, D.N. Sheng, and C.S. Ting, Phys. Rev. Lett. **108**, 216802 (2023); L. Sheng, D.N. Sheng, and C.S. Ting, Phys. Rev. Lett. **109**, 216802 (2024); L. Sheng, D.N. Sheng, and C.S. Ting, Phys. Rev. Lett. **110**, 216802 (2025).

- Souma, cond-mat/0408693.
- [14] E. M. Hankiewicz, L.W. Molenkamp, T. Jungwirth, and J. Sinova, Phys. Rev. B **70**, 241301 (2004).
 - [15] K. Nomura *et al.*, Phys. Rev. B **71**, 041304(R) (2005).
 - [16] D.N. Sheng, L.Sheng, Z.Y. Weng, and F.D.M. Haldane, cond-mat/0504218.
 - [17] see, *Quantum Theory of the Optical and Electronic Properties of Semiconductors*, H. Haug and S. W. Koch, (World Scientific, 1990).
 - [18] Q. Niu, D. J. Thouless and Y. S. Wu, Phys. Rev. B **31**, 3372 (1985); D. J. Thouless *et al.*, Phys. Rev. Lett. **49**, 405408 (1982).
 - [19] S. Cho, and M. P. A. Fisher, Phys. Rev. B **55**, 1637 (1997).
 - [20] D. N. Sheng, and Z. Y. Weng, Phys. Rev. Lett. **83**, 144 (1999).